

# Observation of Non-Vanishing Optical Helicity in Thermal Radiation from Symmetry-Broken Metasurfaces

Xueji Wang<sup>\*,†</sup>, Tyler Sentz<sup>\*,†</sup>, Sathwik Bharadwaj<sup>†</sup>, Subir Ray<sup>†</sup>, Yifan Wang<sup>†</sup>,  
Dan Jiao<sup>†</sup>, Limei Qi<sup>‡</sup>, and Zubin Jacob<sup>\*,†</sup>

<sup>†</sup>*Elmore Family School of Electrical and Computer Engineering, Purdue University, West  
Lafayette, Indiana, 47907, USA*

<sup>‡</sup>*School of Electronic Engineering, Beijing University of Posts and Telecommunications,  
Beijing, 100876, China*

E-mail: zjacob@purdue.edu

\*These authors contribute equally to this work

## Abstract

Spinning thermal radiation is a unique phenomenon that has been observed in many astronomical objects. Investigating the photon spin characteristic in thermal radiation is of general interest and vital importance as it contains exclusive information regarding the emitters. Here, utilizing spin-polarized angle-resolved thermal emission spectroscopy (SPARTES), we study the photon spin in thermal radiation emanating from symmetry-broken metasurfaces. We design metasurfaces that break both inversion- and mirror- symmetries and obtain a unique spin-polarized dispersionless band. We explicitly prove that the summation of spin angular momentum (SAM) projected on wavevectors, namely the optical helicity, is non-vanishing even without

applying a magnetic field. We show the non-vanishing optical helicity is a manifestation of high-purity and highly omnidirectional circular polarization at the dispersionless band, where our design reaches 39% of the fundamental limit. Furthermore, we achieve effective control of the photon spin and the energy-momentum dispersion through symmetry engineering. We demonstrate metasurfaces can impart spin coherence in the incoherent radiation excited by thermal fluctuations. Our results firmly suggest the symmetry-based strategy provides a general pathway for comprehensively controlling the temporal, spatial, and especially spin coherence of thermal radiation.

## Main

Thermal radiation describes the universal phenomenon that all objects at non-zero temperatures emit infrared electromagnetic energy.<sup>1,2</sup> Significant research progress has been made so far in tailoring its temporal coherence, i.e. spectrum,<sup>3-8</sup> and the spatial coherence, i.e. directivity.<sup>9,10</sup> However, the photon spin, another crucial characteristic of electromagnetic radiation, is commonly ignored, since most thermal emitters show weak to zero SAM. Expanding our view to the vast universe, surprisingly, the thermal radiation of many astronomical objects possesses significant circular polarization. The unique phenomenon provides strong evidence for the presence of a magnetic field around some stars,<sup>11</sup> or reveals the existence of chiral organic molecules.<sup>12</sup> Remarkably, recent studies also show that circular polarization can be a possible sign of life.<sup>13</sup> Therefore, revealing photon spin characteristics in thermal radiation is of general interest as it contains exclusive information regarding the emitters.

On the other hand, we point out that the generation of circularly polarized thermal radiation is also important from an engineering perspective. Considering how circularly polarized light is generated in laboratories, the current approach usually requires large benchtop light sources and bulky optical components including linear polarizers and waveplates. Moreover, conventional waveplates are severely compromised by the strong angular dependence, which limits the circular polarization to the proximity of surface-normal. So far, an omnidirectional

circularly polarized light source is still not easily accessible, especially in the mid-infrared region. A tailored thermal radiative source with high-purity and omnidirectional circular polarization can provide an advantageous solution to this long-standing problem.

It is worth noting that recent theoretical explorations predict the thermal radiation from novel materials exhibits circularly polarized characteristics, including hyperbolic materials,<sup>14</sup> magneto-optical materials,<sup>15</sup> Weyl semimetals,<sup>16</sup> and topological insulators.<sup>17,18</sup> Severe unfavorable factors, however, restrict their implementation in practical applications. In some of the materials, a strong magnetic field is required to activate the circular polarization. In other magnetic-field-free cases, the circularly polarized thermal radiation is limited to specific angles or the overall purity is very small. The optical helicity, as a summation of the projected SAM over the far-field hemisphere, is always zero/near-zero. We emphasize that, until now, a direct experimental demonstration of non-vanishing optical helicity in thermal radiation is still missing.

Nevertheless, a high optical helicity, as a manifestation of high-purity and omnidirectional circular polarization, is an attractive attribute to boost the applications of thermal radiation. The photon spin, especially its intertwined characteristics with spectrum and directivity, also introduces a brand new degree of freedom for tailoring thermal radiation (Fig. 1a-d). Thus, to overcome the limitations, we design electromagnetic metasurfaces by engineering the symmetries. Firstly, we note that the photon spin has to degenerate when both inversion- and mirror- symmetries are preserved, and no circularly polarized radiation is observed as illustrated in Fig. 1e. Secondly, by breaking the inversion symmetry, anti-symmetric spin characteristics have been observed.<sup>19</sup> However, we emphasize that although circularly polarized thermal radiation is generated in this scenario, it only occurs in oblique directions, as the mirror-symmetry guarantees spin degeneration in the surface normal. The anti-symmetric spin pattern also ensures the total optical helicity is zero (Fig. 1f). Lastly, we show here the further breaking of mirror-symmetry releases all the constraints. Remarkably, we obtain an asymmetric spin pattern and non-vanishing optical helicity in the radiation

excited by thermal fluctuations (Fig. 1g).

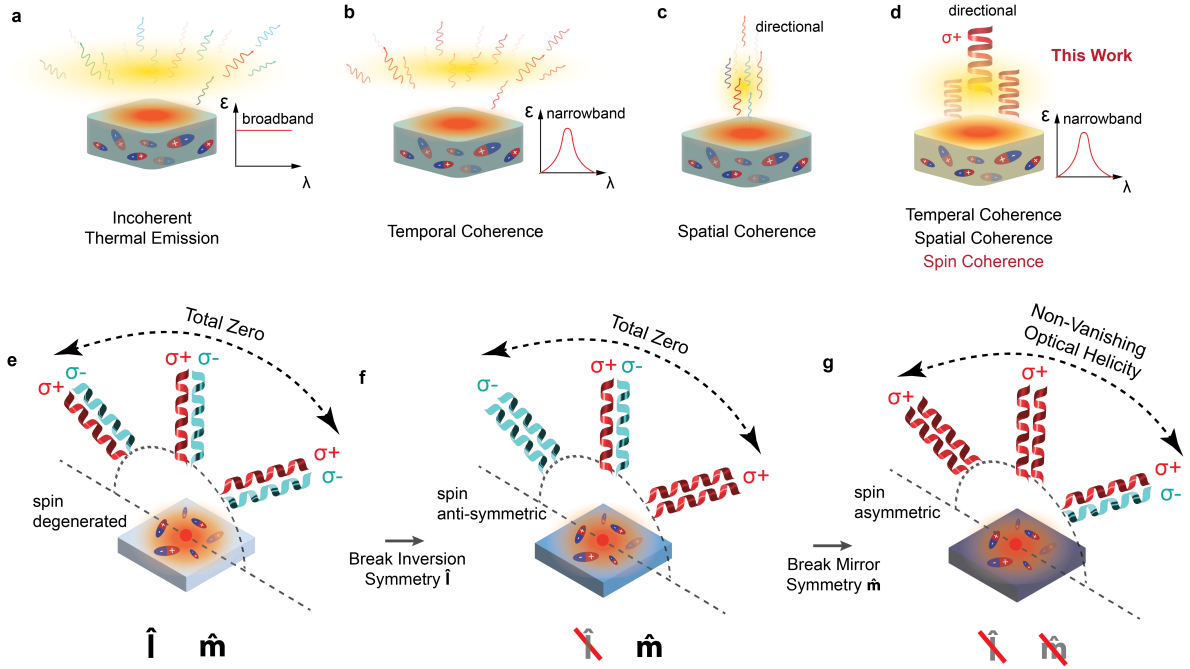


Figure 1: **a-d.** Various aspects of thermal emission engineering. In this work, by adding the optical spin control, we achieve comprehensive tailoring of thermal emission. **e-g.** Schematics demonstrating the constraints of spin degeneracy removal from symmetries. The non-vanishing optical helicity can only be observed when both inversion- and mirror- symmetries are broken (g)

Specifically, in this work, we generate magnetic-field-free circular-polarized thermal radiation with a degree of circular-polarization (DoCP) exceeding 0.6 (DoCP is defined as  $(\sigma_+ - \sigma_-)/(\sigma_+ + \sigma_-)$ , where  $\sigma_+$  and  $\sigma_-$  are the emissivities of left-handed and right-handed circular polarization, respectively). To achieve an omnidirectional high DoCP, we create a spin-polarized dispersionless band around  $7\mu\text{m}$  through the metasurface design. Particularly, based on a thorough characterization using SPARTES, we directly demonstrate the nonvanishing optical helicity in this dispersionless band and show it reaches 39% of the fundamental limit. The complete symmetry breaking in our design also provides full freedom to introduce new symmetries. As some examples, we discuss later three representative configurations with mirror, inversion, and four-fold rotational ( $C_4$ ) symmetries, and show that thermal radiation can be significantly altered by the symmetries. With this symmetry-based

approach, we provide a general and effective pathway to comprehensively engineering the spectral, spatial, and spin characteristics of thermal radiation.

## Spin Degeneracy Removal in Thermal Radiation

To generate the non-vanishing optical helicity, we start by designing a symmetry-broken metasurface that removes spin degeneracy. A schematic of the metasurface is shown in Fig 2a, where a rectangular array of F-shape meta-atoms is patterned on a  $\text{SiO}_2$  dielectric layer with a gold backplane. We point out the 'F' meta-atoms break both inversion- and mirror- symmetry in the pseudo-2D system. The relatively complex structure also provides enough degree of freedom for optimizing the spectrum and band structure. As shown in Fig 2b, the measured emissivity of left-handed circular-polarized light (LCP) is more than 4 times larger than the emissivity of right-handed circular-polarized light (RCP) at the surface normal direction. In Fig 2c, we show a complete characterization of the polarization state based on Stokes parameters. It can be represented by a circular area that is centered close to the north pole of the Poincare sphere (inset of Fig 2c). We emphasize that the near-zero  $S_1$  and  $S_2$  indicate the relatively limited DoCP is actually from the limited coherence of the thermal emission signal.

To show the microscopic mechanisms of the circular polarization and non-vanishing optical helicity, we investigate the near-field electromagnetic response of the metasurface. The major mechanisms of spin degeneracy removal in photonic systems can be divided into two categories. On the one hand, the Pancharatnam-Berry phase generated by a geometric gradient can lead to spin-dependent photon behaviors.<sup>20,21</sup> On the other hand, the phenomenon can also originate from the intrinsic local chirality in the meta-atoms.<sup>22-25</sup> We reveal that the strong intrinsic local chirality of our F-shape plasmonic meta-atoms is the origin of the observed circular-polarized thermal radiation in the far-field. To start with, we calculate the electric field distribution using the finite element method (FEM). The normalized electric

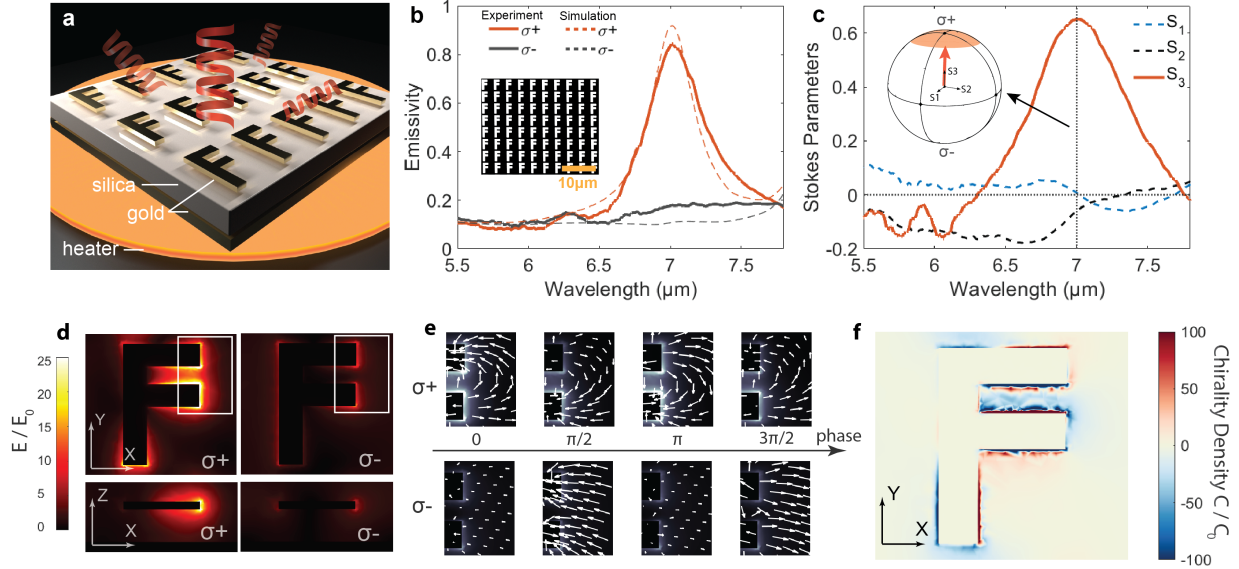


Figure 2: **a.** Schematic of the symmetry-broken metasurface with F-shape meta-atoms. **b.** The measured LCP ( $\sigma+$ ) and RCP ( $\sigma-$ ) emissivity (solid) of the fabricated devices, which show good agreement with the simulation results (dashed). Inset: SEM imaging of the fabricated device. (Scale bar:  $10\mu\text{m}$ ) **c.** Stokes parameters show the full polarization state. Inset: representation of the polarization state in the Poincare sphere. **d.** The time-averaged electric field strength (normalized by the field  $E_0$  of incident waves) at  $7\mu\text{m}$  under LCP (left) and RCP (right) excitations. The fields are plotted along the XY (top) and XZ (bottom) planes, respectively. **e.** Evolution of the vector electric field is plotted for the boxes in **d.** The field is significantly circularly polarized under LCP excitation (top), while it is more linearly polarized under RCP excitation (bottom). **f.** The local optical chirality density  $C$ , normalized by  $C_0$  of the incident LCP.

field strength at  $7\mu\text{m}$  under LCP and RCP excitations are plotted in Fig 2d. An evident resonant enhancement can be observed for LCP excitation near the region of the two horizontal lines of ‘F’, while the enhancement is clearly absent for RCP excitation. The spin-selective resonance is the direct reason for the LCP emissivity peak at  $7\mu\text{m}$ . For more insights, we plot in Fig 2e the vector electric field at different phases. We show the electric field is significantly more chiral under LCP excitation (top) compared with RCP excitation (bottom). Here, to quantitatively characterize the chiral feature of the near-field, we use optical chirality density  $C$ ,<sup>26</sup> as  $C \equiv \frac{\varepsilon_0}{2} \mathbf{E} \cdot \nabla \times \mathbf{E} + \frac{1}{2\mu_0} \mathbf{B} \cdot \nabla \times \mathbf{B}$ , where  $\mathbf{E}$  and  $\mathbf{B}$  are the time-dependent electric and magnetic fields, and  $\varepsilon_0$  and  $\mu_0$  are the permittivity and permeability of vacuum. We emphasize that the local chirality is two orders of magnitude larger than the chirality of the incident LCP as shown in Fig 2f. The super-chiral near-field under LCP excitation is a manifestation of a strong LCP absorption/emission, and at the same time indicates the intrinsic local chirality is the dominant mechanism for our observation of circular-polarized thermal radiation.

## Spin-Polarized Angle-resolved Thermal Emission Spectroscopy

To demonstrate the non-vanishing optical helicity and map the energy-momentum ( $E - k$ ) dispersion of thermal radiation, we establish a unique SPARTES system. The system allows us to characterize the spectral and polarimetric properties of thermal radiation signals at all azimuth ( $\phi$ ) and deflection angles ( $\theta$ ) over the entire far-field hemisphere as shown in Fig. 3a. (The detailed description of the SPARTES system and full thermal emission spectroscopy data can be found in supplementary section II.) In the following, we consider the experimental data along  $k_x$  for our discussion ( $k_y = 0$ ). The measured spectra are plotted in Fig. 3h-k and show an excellent agreement with simulations (Fig. 3d-g). A strong contrast between the emissivity of LCP and RCP is observed, which is a direct manifestation of the spin

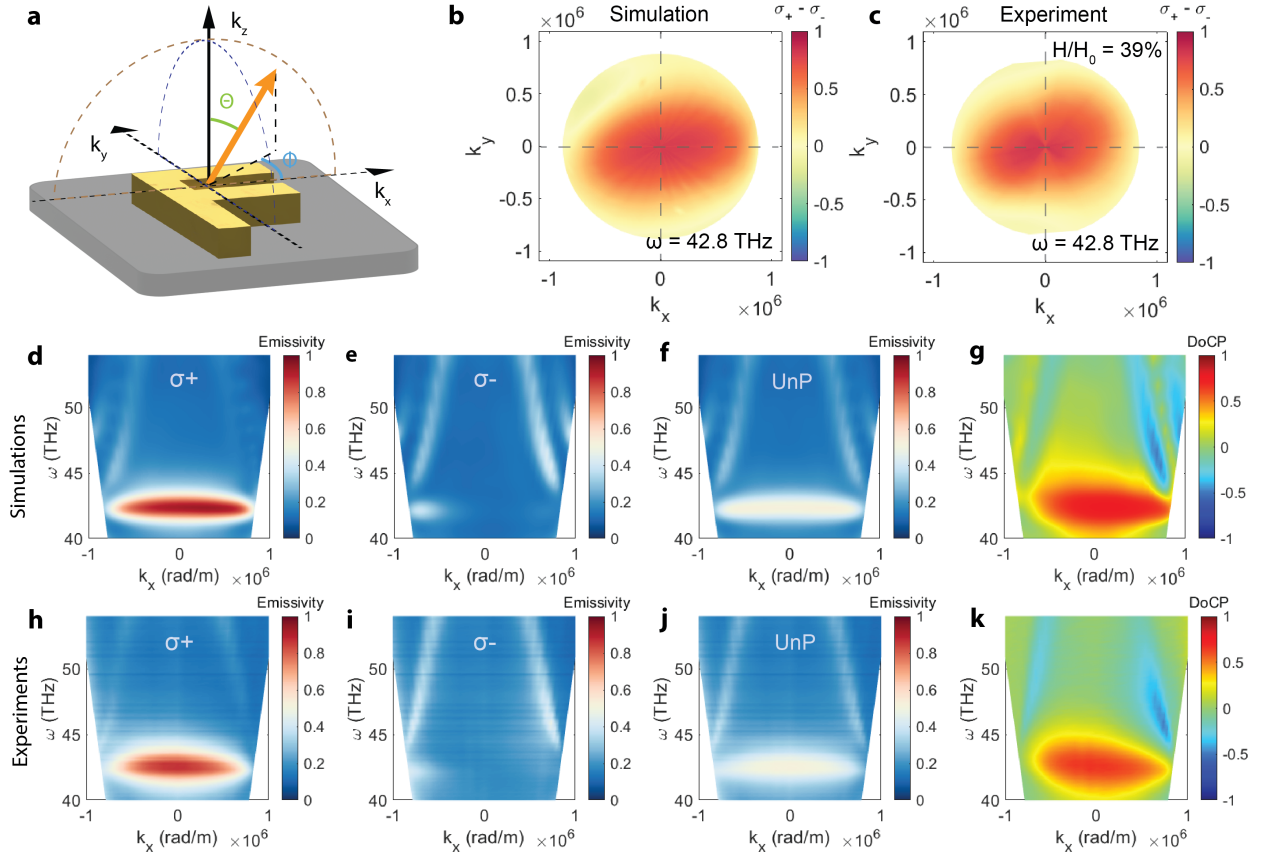


Figure 3: Spin-polarized angle-resolved thermal emission spectroscopy (SPARTES) **a**. Schematic of the coordinate system. **b-c**. Calculated (b) and experimentally measured (c) differential emissivity at 7 microns. The thermal radiation is predominantly LCP over the entire hemisphere. The total optical helicity, which is proportional to the integral of the differential emissivity in the  $k$ -space, is non-zero. It reaches more than one third of the fundamental limits ( $H/H_0=39\%$ ). **d-k**. Simulated (top) and measured (bottom) angle-resolved thermal radiation spectra in the energy-momentum space ( $k_y = 0$ ). The LCP emissivity (d, h), RCP emissivity (e, i), unpolarized emissivity (f, j), and DoCP (g, k) are plotted for comparison. A unique spin-polarized dispersionless band and the spin asymmetry can be clearly observed.

degeneracy removal.

Despite the LCP and RCP emissivities being asymmetric in  $+k$  and  $-k$  by themselves, we note that there is a clear symmetric pattern of the averaged emissivity  $(\sigma_+/2 + \sigma_-/2)$ . This is because the averaged emissivity is proportional to the total radiative power, and the symmetric total radiation in k-space is fundamentally guaranteed by the time-reversal symmetry in this magnetic-field-free system. The asymmetric LCP and RCP emissivity also leads to a unique DoCP pattern, which is neither symmetric nor anti-symmetric. We point out that this spin asymmetry in k-space is from the complete symmetry breaking of our ‘F’ structure, where neither the 2D inversion-symmetry nor the mirror-symmetry is preserved.

Remarkably, we demonstrate that the strong thermal emission at  $7\mu\text{m}$  is from a dispersionless energy band along  $k_x$ . To reveal the thermal radiation characteristics in this dispersionless energy band, we plot the differential circular-polarized emissivity  $(\sigma_+ - \sigma_-)$  at  $7\mu\text{m}$  on the far-field hemisphere (projected onto the  $k_{xy}$  plane). As evidently illustrated in Fig. 3b and Fig. 3c, the thermal radiation is predominantly left-handed circularly polarized in all directions. The total optical helicity  $H$  is nonzero, which is defined as,<sup>27</sup>

$$H = \sum_k \hbar (n_{k,\sigma_+} - n_{k,\sigma_-}) \propto \sum_k (\sigma_+ - \sigma_-) \quad (1)$$

where  $n_{k,\sigma_+}$  and  $n_{k,\sigma_-}$  are the photon numbers of LCP and RCP associated with the wavevector  $k$ .

To explore the fundamental limit, we normalize the optical helicity  $H$  of our device by the optical helicity  $H_0$  of a perfect omnidirectional LCP emitter. We show our design reaches  $H/H_0 = 39\%$  of the fundamental limit from the experimental results. This is in strong contrast with previous demonstrations, where the spin characteristics are anti-symmetric in k-space ( $n_{\sigma_+}(k) = n_{\sigma_-}(-k)$ ) because of the preservation of mirror symmetry, and the optical helicity has to sum to zero.<sup>19</sup> We emphasize the breaking of mirror symmetry in the metasurface is the fundamental mechanism for this observation of non-zero optical helicity

in the radiation excited by thermal fluctuations.

## Symmetry Engineering

Now, we show that the spin characteristics of thermal photons are explicitly governed by the symmetries of the metasurface. We emphasize that we design the ‘F’ structure to have complete symmetry breaking. None of the mirror symmetry, inversion symmetry, or high-order rotational symmetries are present in the meta-atoms, which provides full freedom for symmetry engineering. In other words, by introducing new symmetries, we demonstrate effective control of thermal radiation is realized in its spectral, spatial, and especially spin properties. To show this, in Fig. 4, we present the  $E - k$  dispersion along  $k_y$  ( $k_x = 0$ ) of the averaged emissivity and the corresponding DoCP in three different metasurfaces with mirror, inversion, and 4-fold rotational symmetries (C4), respectively. We point out three interesting features in the obtained thermal emission spectra. Firstly, by introducing mirror-symmetry, the DoCP becomes zero, as the symmetry along y-axis guarantees  $\text{DoCP} = 0$  at  $k_x = 0$ , regardless the value of  $k_y$ . Secondly, we show that the DoCP in the inversion-symmetric device becomes symmetric in the k-space, which is in strong contrast to the ‘single-F’ metasurface where the DoCP is asymmetric. Thirdly, the C4 device also exhibits symmetric patterns, as in 2D, the C4 symmetry contains the inversion symmetry (equivalent to C2 in this 2D case). However, distinctive spectral, spatial, and spin features are present as a manifestation of the additional rotation symmetry. All averaged emissivity plots show symmetric patterns in k-space, which guarantees the time-reversal symmetry is always preserved in our devices.

## Discussion

Finally, we discuss the impact and potential applications of our results. The observed non-vanishing optical helicity indicates highly omnidirectional and even broadband circularly polarized thermal emitters can be realized through metasurfaces. Our demonstrated devices

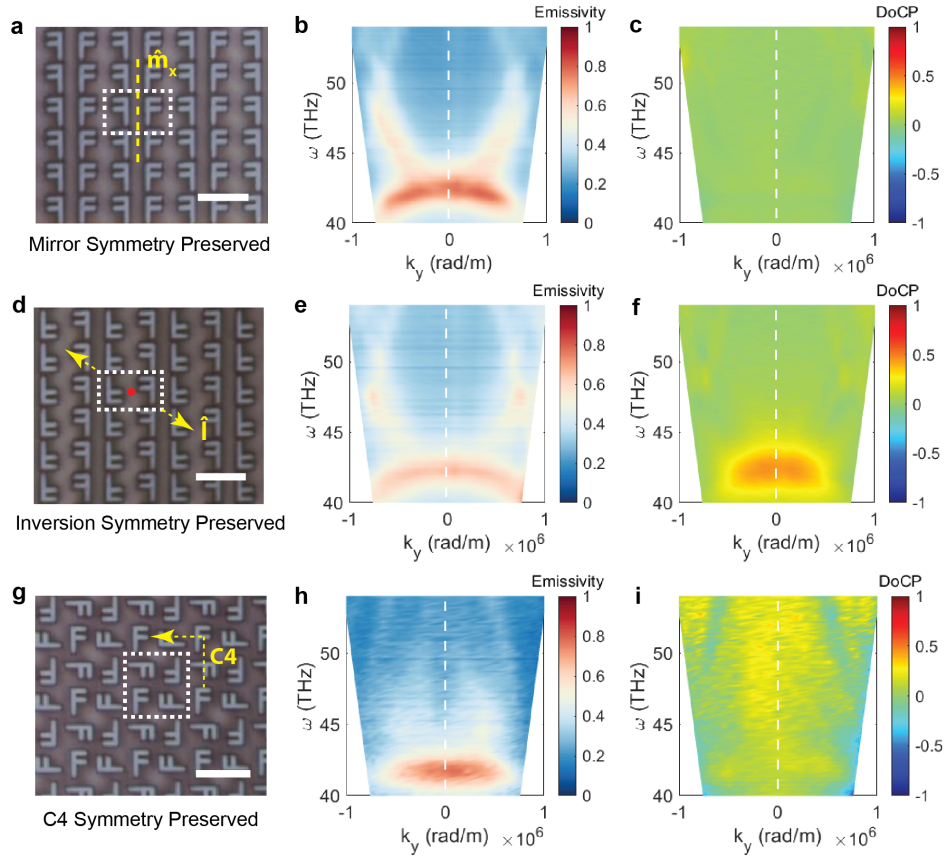


Figure 4: The optical images (left, scale bar:  $5 \mu\text{m}$ ), averaged emissivity spectra (middle), and DoCP are plotted for devices with mirror symmetry (a-c), inversion symmetry (d-f), and four-fold rotational symmetry (g-i), respectively. The average emissivity is symmetric along  $k=0$  in all three cases, which is a manifestation of the time-reversal symmetry. The DoCP is zero for the mirror-symmetric device, and symmetric for the inversion- and C4- devices.

here can be directly applied as a wide-angle, narrow-band circular-polarized mid-infrared light source, for applications including optical gas sensing, illumination, and display. We highlight that the metasurface-based device can be integrated into on-chip systems to achieve compact functional devices for commercialization. Moreover, considering the field of near-field heat transfer, we expect a thermal emitter with non-vanishing optical helicity can transfer net angular momentum and torque through heat. Although more detailed analysis is undoubtedly required, the exploration in this direction may facilitate the discovery of novel phenomena at the nanoscale, and eventually, benefit the development of near-field thermophotovoltaics. Additionally, the unique spectral-spatial-spin feature of the engineered thermal emission can be exploited as high-contrast infrared beacons, as the thermal emission from other natural objects is highly incoherent, without any spin textures. Finally, our metasurface-based strategy for controlling optical spin introduces a new degree of freedom of thermal radiation engineering, providing a general approach to comprehensively tailoring thermal radiation for future energy applications.

## **Data Availability**

The data that supports this paper and other findings are available from the corresponding author on reasonable request.

## **Acknowledgments**

The authors thank F. Kalhor for useful discussions. The authors thank A. Jishi for experimental assistance. The authors thank the Defense Advanced Research Projects Agency (DARPA) Nascent Light-Matter Interactions (NLM) for funding to pursue this research.

# Competing Interests

The authors declare no competing interests.

## References

- (1) Baranov, D. G.; Xiao, Y.; Nechepurenko, I. A.; Krasnok, A.; Alù, A.; Kats, M. A. Nanophotonic engineering of far-field thermal emitters. *Nat. Mater.* **2019**, *18*, 920–930.
- (2) Fan, S. Thermal photonics and energy applications. *Joule* **2017**, *1*, 264–273.
- (3) Greffet, J.-J.; Carminati, R.; Joulain, K.; Mulet, J.-P.; Mainguy, S.; Chen, Y. Coherent emission of light by thermal sources. *Nature* **2002**, *416*, 61–64.
- (4) Asano, T.; Suemitsu, M.; Hashimoto, K.; De Zoysa, M.; Shibahara, T.; Tsutsumi, T.; Noda, S. Near infrared to visible highly selective thermal emitters based on an intrinsic semiconductor. *Sci. Adv.* **2016**, *2*, e1600499.
- (5) Dyachenko, P. N.; Molesky, S.; Petrov, A. Y.; Störmer, M.; Krekeler, T.; Lang, S.; Ritter, M.; Jacob, Z.; Eich, M. Controlling thermal emission with refractory epsilon-near-zero metamaterials via topological transitions. *Nat. Commun.* **2016**, *7*, 11809.
- (6) Yeng, Y. X.; Ghebrebrhan, M.; Bermel, P.; Chan, W. R.; Joannopoulos, J. D.; Soljačić, M.; Celanovic, I. Enabling high-temperature nanophotonics for energy applications. *Proc. Natl. Acad. Sci.* **2012**, *109*, 2280–2285.
- (7) Liu, X.; Tyler, T.; Starr, T.; Starr, A. F.; Jokerst, N. M.; Padilla, W. J. Taming the Blackbody with Infrared Metamaterials as Selective Thermal Emitters. *Phys. Rev. Lett.* **2011**, *107*, 045901.

- (8) De Zoysa, M.; Asano, T.; Mochizuki, K.; Oskooi, A.; Inoue, T.; Noda, S. Conversion of broadband to narrowband thermal emission through energy recycling. *Nature Photonics* **2012**, *6*, 535–539.
- (9) Park, J. H.; Han, S. E.; Nagpal, P.; Norris, D. J. Observation of thermal beaming from tungsten and molybdenum bull’s eyes. *ACS Photonics* **2016**, *3*, 494–500.
- (10) Xu, J.; Mandal, J.; Raman, A. P. Broadband directional control of thermal emission. *Science* **2021**, *372*, 393–397.
- (11) De, S.; Tashiro, H. Circular Polarization of the CMB: A probe of the First stars. *Physical Review D* **2015**, *92*, 123506.
- (12) Bailey, J.; Chrysostomou, A.; Hough, J.; Gledhill, T.; McCall, A.; Clark, S.; Ménard, F.; Tamura, M. Circular polarization in star-formation regions: Implications for biomolecular homochirality. *Science* **1998**, *281*, 672–674.
- (13) Sparks, W.; Hough, J. H.; Germer, T. A.; Robb, F.; Kolokolova, L. Remote sensing of chiral signatures on Mars. *Planetary and Space Science* **2012**, *72*, 111–115.
- (14) Khandekar, C.; Khosravi, F.; Li, Z.; Jacob, Z. New spin-resolved thermal radiation laws for nonreciprocal bianisotropic media. *New Journal of Physics* **2020**, *22*, 123005.
- (15) Ott, A.; Ben-Abdallah, P.; Biehs, S.-A. Circular heat and momentum flux radiated by magneto-optical nanoparticles. *Physical Review B* **2018**, *97*, 205414.
- (16) Wang, Y.; Khandekar, C.; Gao, X.; Li, T.; Jiao, D.; Jacob, Z. Broadband circularly polarized thermal radiation from magnetic Weyl semimetals. *Optical Materials Express* **2021**, *11*, 3880–3895.
- (17) Maghrebi, M. F.; Gorshkov, A.; Sau, J. Fluctuation-induced torque on a topological insulator out of thermal equilibrium. *Physical review letters* **2019**, *123*, 055901.

- (18) Khan, E.; Narimanov, E. E. Spinning radiation from a topological insulator. *Physical Review B* **2019**, *100*, 081408.
- (19) Shitrit, N.; Yulevich, I.; Maguid, E.; Ozeri, D.; Veksler, D.; Kleiner, V.; Hasman, E. Spin-optical metamaterial route to spin-controlled photonics. *Science* **2013**, *340*, 724–726.
- (20) Yin, X.; Ye, Z.; Rho, J.; Wang, Y.; Zhang, X. Photonic spin Hall effect at metasurfaces. *Science* **2013**, *339*, 1405–1407.
- (21) Nalitov, A.; Malpuech, G.; Terças, H.; Solnyshkov, D. Spin-orbit coupling and the optical spin hall effect in photonic graphene. *Physical review letters* **2015**, *114*, 026803.
- (22) Hentschel, M.; Schäferling, M.; Duan, X.; Giessen, H.; Liu, N. Chiral plasmonics. *Science advances* **2017**, *3*, e1602735.
- (23) Hendry, E.; Carpy, T.; Johnston, J.; Popland, M.; Mikhaylovskiy, R.; Laphorn, A.; Kelly, S.; Barron, L.; Gadegaard, N.; Kadodwala, M. Ultrasensitive detection and characterization of biomolecules using superchiral fields. *Nature nanotechnology* **2010**, *5*, 783–787.
- (24) Mahmud, M. S.; Rosenmann, D.; Czaplewski, D. A.; Gao, J.; Yang, X. Chiral plasmonic metasurface absorbers in the mid-infrared wavelength range. *Optics Letters* **2020**, *45*, 5372–5375.
- (25) Gansel, J. K.; Thiel, M.; Rill, M. S.; Decker, M.; Bade, K.; Saile, V.; von Freymann, G.; Linden, S.; Wegener, M. Gold helix photonic metamaterial as broadband circular polarizer. *Science* **2009**, *325*, 1513–1515.
- (26) Tang, Y.; Cohen, A. E. Optical chirality and its interaction with matter. *Physical review letters* **2010**, *104*, 163901.

- (27) Cameron, R. P.; Barnett, S. M.; Yao, A. M. Optical helicity, optical spin and related quantities in electromagnetic theory. *New Journal of Physics* **2012**, *14*, 053050.